 FDMP, vol.8, no.2, pp.173-195, 2012

# Thermal Effects on the Spreading and Solidification of a Micrometric Molten Particle Impacting onto a Rigid Substrate

**S. Oukach[1,2,3], H. Hamdi[2], M. El Ganaoui[4] and B. Pateyron[1]**

**Abstract:** The splat formation is one of the basic processes in thermal spray coatings. The performance of these coatings is strongly related to the process of spreading and solidification of molten droplets. The aim of the present paper is to simulate the fluid flow, heat transfer and phase-change that occur when a micrometric molten droplet impacts onto a rigid substrate and to examine the effect of the substrate conditions, such as initial temperature and material on the solidification time and spreading process. The effect of thermal contact resistance is also investigated. The simulation model used is based on the Navier-Stokes equations and the energy equation which includes convection and phase change. These equations are coupled with the Level Set function to track the interface between molten particle and surrounding air. The numerical model is solved using Finite Element Method and Comsol multiphysics 3.5a software.

**Keywords:** droplet impact, solidification, multiphase flow, level set, and thermal contact resistance.

## 1 Introduction

Despite of being studied over a century [Worthington (1876),Worthington (1877)], the process of droplets impingement on solids surfaces continues to be a challenging problem for engineers and scientists due to its relevance to many industrial and engineering applications such as thermal spray, fuel combustion, ink-jet printing, painting and so on. In thermal spray technology, coatings are obtained by injecting

[1] Laboratory of Science of Ceramic Processes and Surface Treatments, (SPCTS UMR 6638 CNRS), University of Limoges, Limoges, France
[2] Laboratory of Fluid Mechanics and Energetic (LMFE URAC 27 CNRST), FSSM, Cadi Ayyad University, Marrakech, Morocco
[3] soufiane.oukach@etu.unilim.fr
[4] Laboratory of Studies and Research on Wood (LERMAB), Institut Carnot, Henri Poincaré University, Nancy, France

material (as powder or particles) into a plasma jet in which the particles are melted and projected at high speed toward a prepared surface on which they flatten, quench rapidly and solidify. Coating is formed when millions of particles are cumulatively deposited on the top of each other layer by layer, which leads to a lamellar structure [Fauchais P. (2003)].Thermal sprayed coatings are extensively used in a wide variety of applications including aerospace, automotive and electronic/semiconductor to increase components life and improve their performances. Many studies have shown that the microstructure and physical properties of coatings, which condition their quality and performance, are strongly related to the process of splat formation. A better understanding of the parameters that govern the deposition and solidification of an individual molten particle and thus the splat formation will help improve the quality and microstructure of the coatings.

The process of droplet spreading and solidification has received substantial attention in the literature. Madejski [Madejski (1976)] investigated the solidification of droplets. He assumed that the splat takes the form of a disk after impact. Using a simple energy conservation, he found an analytical solution to one dimensional Stefan problem.

Experimental studies have focused on the impact of molten droplets on substrates by using high speed cameras with short exposure time [Cedelle J, (2004)]. The effects of impact angle and viscosity on droplet impact behavior were investigated by Sikalo et al [Sikalo, Tropea and Ganic (2005)]. Using low impact angles, they have shown that the deposition ratio (ratio of the amount of deposited liquid to the total amount of liquid impacting on the substrate) is governed by the droplet size and the normal velocity. Mundo et al. [Mundo, Sommerfeld and Tropea (1995)] have shown that the substrate roughness has an important effect on the droplet dynamics. Fukai et al. [Fukai (1995)] have found that impact velocity has a significant effect on the droplet spreading especially for limited wetting.

Numerical models have been developed to investigate the important phenomena occurring during the droplet impact and deposition. Harlow and Shannon [Harlow and Shannon (1967)] were the first to simulate droplet impact on a solid surface by using "marker-and-cell" (MAC) finite-difference method. In this first model, the effects of viscosity and surface tension have been neglected.

The MAC model was then enhanced by Tsurutani et al [Tsurutani, Yao, Senda and Fujimoto (1990)] taking into account the effects of surface tension and viscosity and also the heat transfer between droplet and surface that occurs during its spreading. Fukai et al [Fukai, Zhao, Poulikakos, Megaridis and Miyatake (1995)] used a finite element method to study droplet deposition by assuming that solidification starts after the end of spreading.

Bianchi et al [Bianchi et al (1994)] and Fukumoto et al [Fukumoto, Katoh and Okane (1995)] have shown that the initial substrate temperature has a significant effect on the splat morphology and consequently on the microstructure and quality of the coating. The splat morphology has been found to change with the substrate temperature. Cold substrates result in splat fragmentation while hot substrates lead to splats holding a disk shape.

Although the thermal contact resistance between the droplet and the substrate has a significant effect in the solidification process [Trapaga et al (1992), Pasandideh-Fard and Mostaghimi (1996)], it has been neglected in most studies mentioned above and also in other ones [Liu, Lavernia and Rangel (1993), Bertagnolli, Marchese and Jacucci(1995)].

The aim of the present paper is to model and simulate the process of impact and spreading of a micrometric alumina particle impacting with a low velocity onto a substrate taking into account the solidification process. The simulation aims to study the effect of the important parameters which govern the splat formation such as, initial substrate temperature, substrate material and thermal contact resistance on the spread factor and the solidification process.

The properties of the particle at the end of its flight in the plasma flame: velocity and temperature, are used as impact velocity and initial particle temperature. They are evaluated according to the characteristics of the plasma jet: power, gas flow, nozzle diameter, speed and initial position of the particle feed [Ettouil, F.B., (2008), Delluc, G. (2005)]. For these calculations, knowledge of thermodynamic properties and the plasma gas mixture transportation are crucial [Pateyron, B (1996), Pateyron, B (2005)].

## 2 Numerical model

The process of impact, spreading and solidification of a molten droplet impinging onto a solid surface involves fluid flow, heat transfer and phase change. Complex phenomena involved are yet not thoroughly understood. For example, the interface between the droplet and the surrounding gas and between liquid and solid phases remains a challenging problem to deal with for scientists and engineers.

In the present work, a two-dimensional axi-symmetric model was used to simulate the impingement of an alumina molten particle onto a rigid substrate. The geometry of the problem and the initial configuration are shown in figure1. The geometry contains two domains: the first one contains the droplet and the surrounding gas (air) while the second one contains just the substrate. The equilibrium contact angle is set to $\theta = 70^{\circ}$ [Mebdoua (2008)]. The use of a fixed contact angle under the thermal spray conditions has been justified [Pasandideh-Fard and Mostaghimi

(1994)].

The numerical model is solved using Finite Element Method and Comsol multiphysics 3.5a software. Its validation was presented in former papers [Oukach, El Ganaoui, Hamdi and Pateyron (2010); Oukach, Pateyron, El Ganaoui and Hamdi (2010)].

### *2.1 Flow dynamics*

The fluid flow during the droplet spreading onto the substrate is modeled by using the full Navier-Stokes equations for incompressible flows (Eq.1and Eq.2):

$$\rho\frac{\partial u}{\partial t}+\rho(u.\nabla)u=-\nabla p+\nabla.\mu(\nabla u+(\nabla u)^T)+\rho g+F_{TS}+F \tag{1}$$

$$\nabla.u=0 \tag{2}$$

Where $u$ is the velocity, $p$ the pressure, $\rho$ the density and $\mu$ the kinematic viscosity and$g$ is the gravitational acceleration. $F$ is the term source corresponding to the occurrence of the droplet solidification and $F_{TS}$ represents the capillary forces given by (Eq.3):

$$F_{TS}=\sigma\dot{k}\dot{\delta}\dot{n} \tag{3}$$

Where $\sigma$, $\delta$ and $k$ are respectively the surface tension coefficient, the Dirac function and the average local slop of the curve at the liquid-gas interface. $n$ is the normal at the liquid-gas interface.

Both fluids are assumed incompressible and Newtonian, and the surrounding gas (air) has no effect on the deposition process.

### *2.2 Advection on the interface*

To track the evolution of the interface between the two fluids (liquid and air), the level set method was used [Sethian (1996), Hogea C.S., Murray B.T., Sethian J.A., (2005), Lowengrub J.S., Xu J-J. and Voigt A., (2007)]. In this method, the interface is represented by a certain level set or iso-contour of a globally defined function: the level set function $\varphi$. This function $\varphi$ is a smoothed step function that equals (0) in a domain and (1) in its complementary part. Across the interface, there is a smooth transition from (0) to (1) and the interface is represented by the 0,5 iso-contour (Fig.1). The interface moves with the fluid velocity $u$. This is described by the following equation (Eq.4):

$$\frac{\partial\phi}{\partial t}+u\dot{\nabla}\phi=\gamma\nabla\dot{(}\varepsilon\nabla\phi-\phi(1-\phi)\frac{\nabla\phi}{|\nabla\phi|}) \tag{4}$$

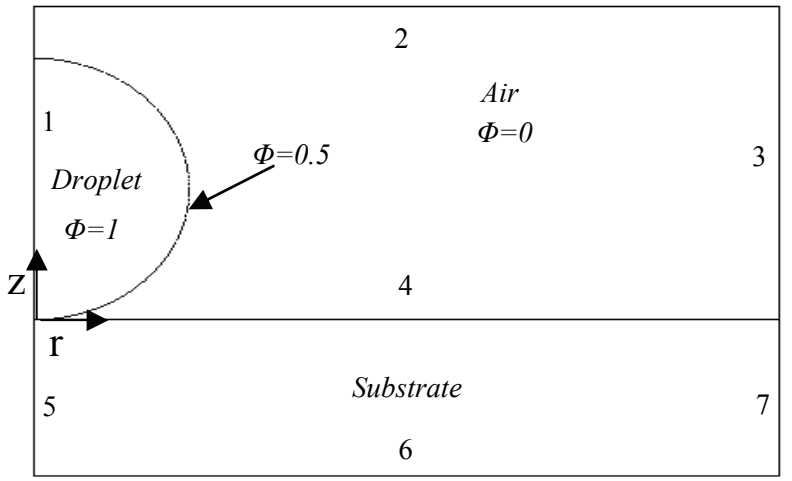


Figure 1: Initial configuration. Numeric labels: 1 to 7 refer to boundaries for which conditions are set on table 1.

The terms on the left-hand side of (Eq.4) give the correct motion of the interface, while those on the right-hand side are necessary for numerical stability. The parameters $\varepsilon$ and $\gamma$ determine the thickness of the region and the amount of re-initialization or stabilization of the level set function respectively. Any property $\alpha$ of the two fluids at the interface such as density, viscosity or thermal conductivity is expressed as (Eq.5):

$$\alpha = \alpha_{gas} + \phi(\alpha_{1iquid} - \alpha_{gas}) \tag{5}$$

### *2.3 Heat transfer and solidification*

The heat exchange between the droplet, air and substrate is modeled by using the energy equation (Eq.6):

$$\rho C_p \frac{\partial T}{\partial t} + \nabla \cdot (-\lambda \nabla T) = -\rho C_p \mathrm{u}.\nabla T \tag{6}$$

Where *T,* $\rho$ and $C_p$ denote respectively temperature, density and specific heat. The term on the right hand side is introduced to include the convective heat effects. The energy equation is solved in all domains (Fig.1).

The thermal contact resistance (TCR) is introduced to take into account the discontinuity of temperature at the interface due to the non perfect contact between the droplet and the substrate. TCR is modeled by defining a thin layer of arbitrary thickness $l_0$ which attaches the two domains. The effective thermal conductivity $k_l$ for the splat is related to the TCR by (Eq.7):

$$k_l = \frac{l_0}{TCR} \tag{7}$$

As the hot droplet spreads on the cold substrate, it cools down and solidifies. Many approaches has been used for modeling solid/liquid transitions. The enthalpy porosity method shows a good ability for modeling complex problems involving phase change as crystal growth from the melt (El Ganaoui et Bontoux 1998, El Ganaoui et al 1999, El Ganaoui et al 2002, Prud'homme et El Ganaoui 2006). Here a variant of the enthalpy method is used (Diego Celentano et al, 2011). The specific heat $C_p$ in the energy equation (Eq.6) is replaced by:

$$Cp = Cp_{solide} + \frac{\Delta H}{T_m}.f + \Delta H.\delta \tag{8}$$

Where $f$ is a smooth Dirac delta function with nonzero values in a range of temperature equal to $\Delta T$ and its integration over temperature is equal to unity, $\Delta H$ the latent heat of the transition, $T_m$ the melting temperature. $\Delta T$ is the temperature gap between liquidus temperature ($T_m$+$\Delta T$) and solidus one ($T_m$-$\Delta T$) and $\delta$ is a Gaussian curve given by (Eq.9):

$$\delta = \frac{\exp(-(T-T_m)^2/(\Delta T)^2)}{\Delta T\sqrt{\pi}} \tag{9}$$

The source term in (Eq.1) is defined in (Eq.10) and serves to slow down the velocity of the fluid at the phase-change interface and eventually arrest its motion as the droplet cools down [Voller, Markatos and M. Cross (1985)].

$$F = \frac{(1-\beta)^2}{\beta^3+\eta}.C.u \tag{10}$$

Where $\beta$ is the volume fraction of the liquid phase, given by (Eq.11):

$$\beta = \begin{cases} 0 & T < T_m - \Delta T \\ \frac{T-T_m+\Delta T}{2\Delta T} & T_m - \Delta T \leq T \leq T_m + \Delta T \\ 1 & T > T_m + \Delta T \end{cases} \tag{11}$$

In (Eq10) $C$ is the mushy zone constant (should have high value to produce a proper damping), $\eta$ arbitrary constant (should have small value to prevent division by zero) and $u$ is the spreading velocity of the splat.

### *2.4 Boundary conditions*

The boundary conditions are listed in table 1. The Navier-Stokes equations (Eq.1 and Eq.2) and the level set equation (Eq.4) are active only into the domain which contains the droplet and the surrounding gas (Fig.1). The axial symmetry condition is used on the axis of the droplet which coincides with the axis of symmetry of the geometry. The top and right boundaries in the domain where the droplet and the gas are present (labels 2 and 3 on figure 1) are set to the no slip condition. The wetted wall condition is used for the droplet-substrate boundary (label 4 on figure 1); this condition allows to take into account the wettability by introducing the static contact angle $\theta$.

Concerning the heat flow, the conservation energy equation is applied in all the domains; the axis of the droplet is set to an axial symmetry condition, while the other boundaries (labels 2,3,6 and 7 on figure 1) are set to an isolated boundary condition.

Table 1: Boundary conditions

| Boundary | Navier-Stokes Equations | Heat transfer Equation |
|---|---|---|
| 1 | Axial symmetry | Axial symmetry |
| 2,3 | No slip condition | Insulation |
| 4 | Wetted wall | Insulation |
| 5 | Not active | Axial symmetry |
| 6,7 | Not active | insulation |

## 3 Results and discussions

Results are carried out for an alumina particle of 20$\mu$m diameter with initial temperature of 2800K (well above the melting point of alumina $T_m$=2325K) and impact velocity of 20m/s (to avoid defragmentation and splashing of the splat [Mundo et al (1995)]). The droplet is impinging on various material substrates (aluminum, steel, and alumina) set at various initial temperatures (300K, 500K, and 700K). The two cases of spreading with and without solidification are first compared to investigate the effect of taking into account the process of solidification and then the effects of substrate temperature, substrate material and thermal contact resistance are discussed.

### *3.1 Spreading with and without solidification*

Spreading is evaluated by using the so known spread factor, $\xi = D/D_0$, given by normalizing the splat diameter $D$ to the initial droplet diameter $D_0$.

Figure 2 displays different stages of a 20$\mu$m molten alumina particle impacting onto a steel substrate with a low velocity of 20m/s. The initial temperature of the droplet is 2800K while the initial temperature of the substrate is set to 300K. Thermophysical properties of different materials used in this study are listed in Table 6. In the absence of solidification, when heat effects are considered without any influence on the spreading process (i.e. F=0 in Eq.1), (Fig.2 column (a)), the droplet starts spreading rapidly after impingement on the surface with a radial velocity higher than that before impact; this is characterized by an increase in the spread factor at the early stages of the droplet spreading (Fig.3). This fast spreading is due to the high compression that undergoes the droplet at the impact; a shock wave generates and proceeds upward inside the droplet thus the elastic energy on the compressed liquid is gradually transferred into the kinetic energy of lateral flow [Ivosevic, Richard, Cairncross and Knight (2006)].

After it reaches its maximum spreading (Fig.2 column (a)), at about t=2$\mu$s, the droplet recoils due to the surface tension forces, thus the spread factor decreases rapidly from its maximum which is larger than the equilibrium value to a minimum which is smaller than the equilibrium one (Fig.3), then the droplet exhibits a couple of oscillations involving spreading and recoil before reaching the equilibrium state where its remaining kinetic energy is completely dissipated by the surface tension and viscous forces effects. The diameter of the splat reaches its equilibrium value at approximately 26$\mu$s.

When heat effects are considered by taking into account the damping forces (F$\neq$0 in Eq1), the solidification phenomena has a significant effect on the spreading process, as shown in figure 2 column (b) where the liquid phase is indicated in white while the solidified part of the droplet is indicated in black. After the collision with the rigid substrate, the droplet starts to spread rapidly and cools down. Solidification starts just after collision in the lowest part which is in contact with the substrate, a plateau starts to form and slows down the motion of the fluid phase above. At the end of spreading, the base of the splat is solidified while the portion on the top is still liquid, tends to recoil and subsequently oscillate until its kinetic energy is dissipated by viscous and surface tension forces. The front of solidification continues to progress in the z-axis direction until t=21$\mu$s when the splat is completely solidified. As shown in figure 3, the spread factor reaches its maximum $\xi_{max}$ = 1.93 at about t = 2 $\mu$s (the same in the case without solidification) and remains almost the same because the base of the splat is already solidified.

It can be seen from figure 3 that while the spread factor, in the case without solidification, goes to a maximum value higher than that achieved in the case with solidification, it diminishes to a final value at the end of splat spreading less than the value achieved in the case of solidification. This leads also to different final

thickness of splat. The values of the parameters compared for the two cases are reported in table 2. The most important effects to be pointed out is that the final splat thickness is 28.4% higher and the final splat diameter is 22,3% lower when the solidification effect is not considered. Consequently, the solidification effect has to be taken into account when dealing with splat spreading in thermal deposition.

### *3.2 Effect of substrate temperature*

In order to evaluate the effect of substrate temperature on the droplet spreading and solidification process, a steel substrate was set at different initial temperatures: Ts=300K, 500K and 700K. The thermal contact resistance was held constant and set to TCR=$1.10^{-7}$m$^2$K/W. The process of spreading and solidification is almost the same as described in the above section for the solidification case (Fig2.column (b)). Figure 4 shows the droplet temperature evolution at 1$\mu$m depth location

Table 2: Values of parameters compared for the two cases: with and without solidification

| Parameters \ Cases | Without solidification | With solidification |
|---|---|---|
| Maximum spread factor | 2.32 | 1.93 |
| Final spread factor | 1.5 | 1.93 |
| Splat solidification time (µs) | - | 21 |
| Final spread time (µs) | 26 | 2 |
| Final splat thickness (µm) | 10.2 | 7.3 |

from the substrate surface at the first instants of impact on a steel substrate set at different initial temperatures. It's observed from this figure that increasing the substrate initial temperature leads to slowing the droplet's cooling, for example at t=2.5$\mu$s, the temperature decreases from 2800K (initial temperature) to 2226K for Ts=300K, 2308K for Ts=500K and 2336K for Ts=700K, which means that solidification in the droplet has already begun for Ts=300K and Ts=500K, while for Ts=700K, the droplet is still liquid. This leads to different solidification times for different substrate initial temperature.

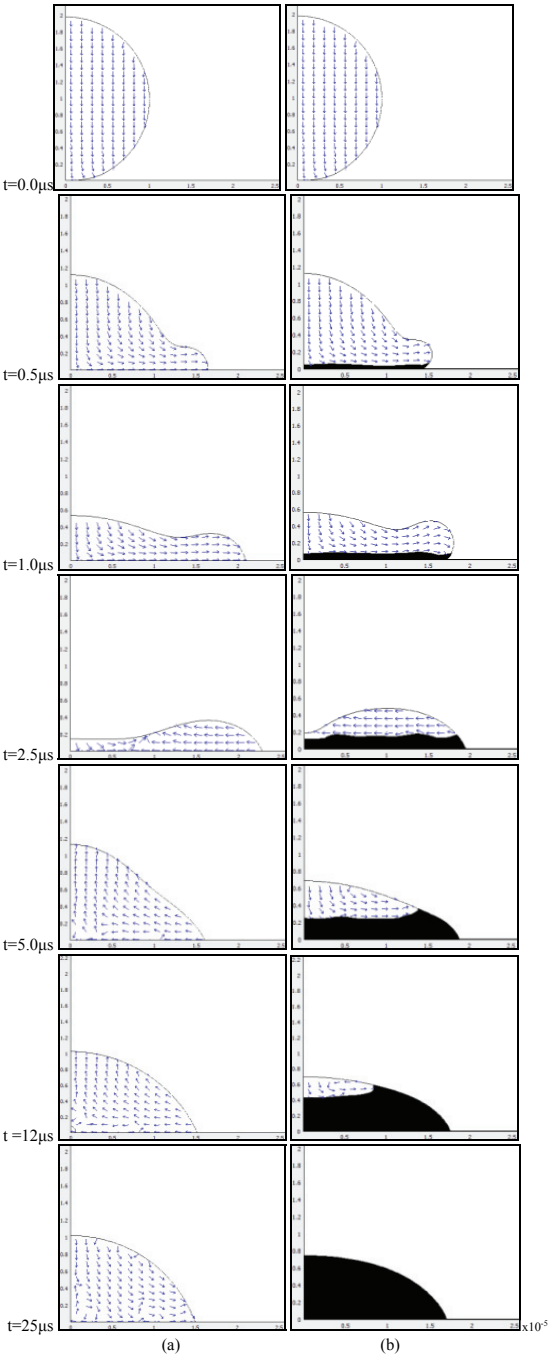


Figure 2: Different stages of a 20$\mu$m molten alumina particle impacting onto a steel substrate: without solidification (a), with solidification (b). The arrows indicate the direction of the liquid motion inside the droplet.

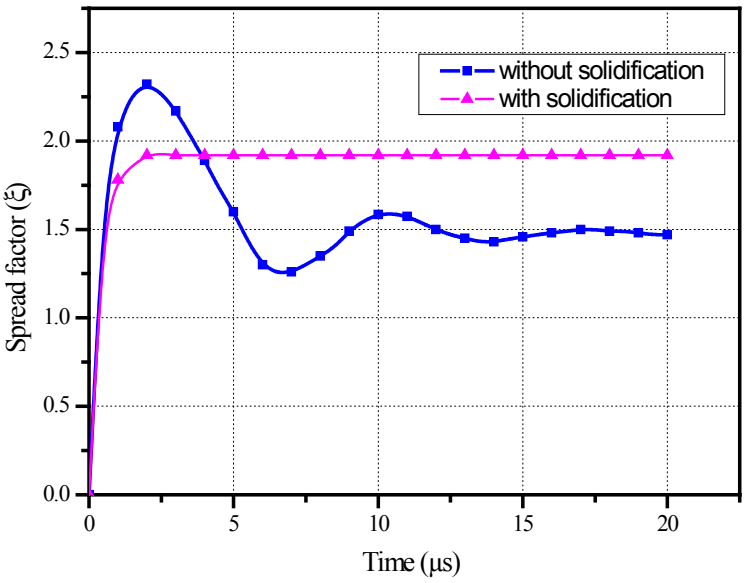


Figure 3: Spread factor evolution during the droplet spreading for the two cases: with and without solidification.

Solidification time is a key factor in thermal spraying. It is influenced by the initial temperature and the nature of the substrate. The computed solidification time as a function of initial temperature and nature of the substrate is shown in Figure 5. It can be seen from this figure that the solidification time is influenced by the substrate initial temperature and that the effect is more important for alumina than for steel substrate, while the effect is weak for aluminum substrate. The droplet solidifies rapidly when the substrate is cold. Indeed, increasing the substrate temperature leads to decrease the temperature gradient between the droplet and the substrate which reduces the heat transfer rate from the droplet to the substrate thus the droplet keeps its thermal energy longer leading to an increase of its solidification time.

The spread factor evolution during the droplet deposition on a steel substrate as a function of time for different initial substrate temperatures is shown in figure 6. At the beginning of spreading, before t=0.5$\mu$s, the evolution of the spread factor is not affected by the substrate temperature while after that time a slight influence of the initial substrate temperature is observed leading to different values of the final spread factor which increases when increasing the substrate initial temperature. The final spread factor, which corresponds to its maximum, is about $\xi_{max}$=1.93 for

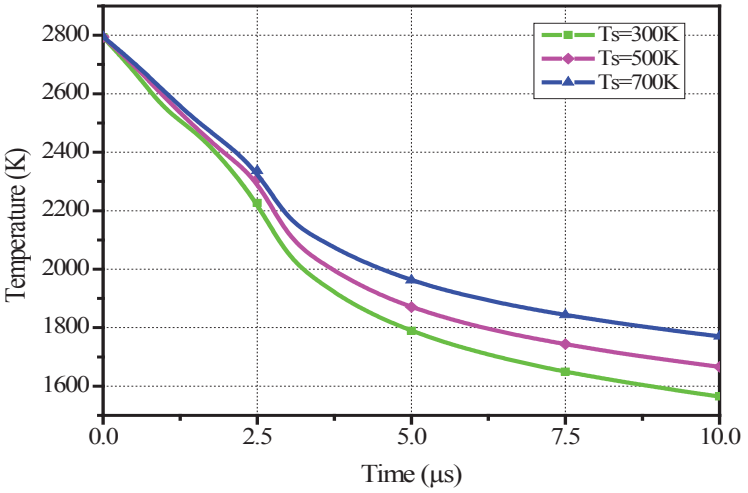


Figure 4: Droplet temperature evolution at 1$\mu$m depth location from the substrate surface (z=1$\mu$m) for different initial substrate (steel) temperatures at the first instants of impact (Ts=300K, Ts=500K and Ts=700K)

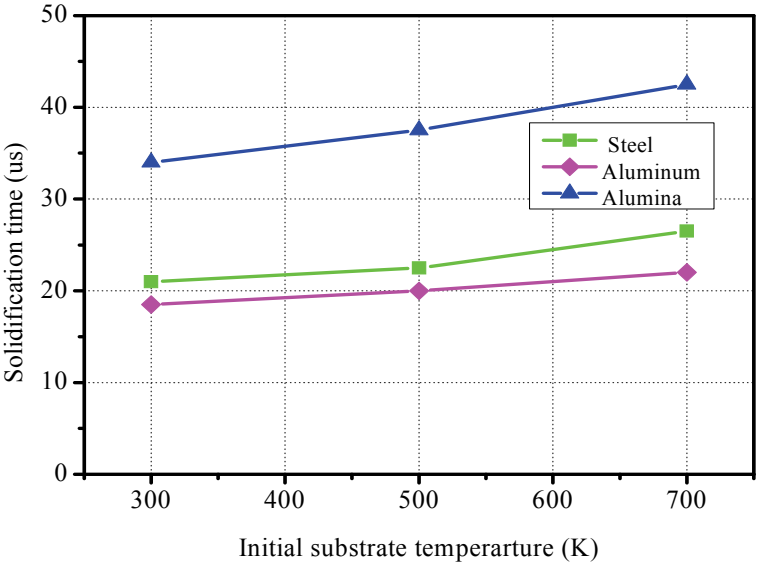


Figure 5: Time of complete solidification for different initial substrate temperatures and different substrate materials

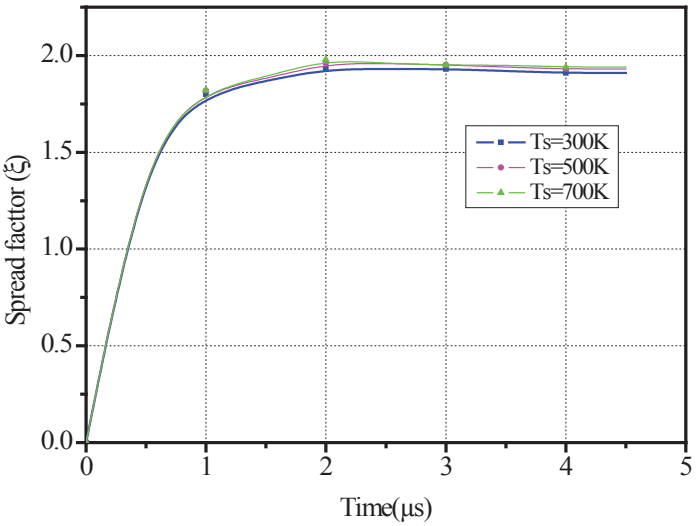


Figure 6: Evolution of spread factor during the droplet spreading for different initial substrate (steel) temperatures (Ts=300k, Ts=500K, and Ts=700K).

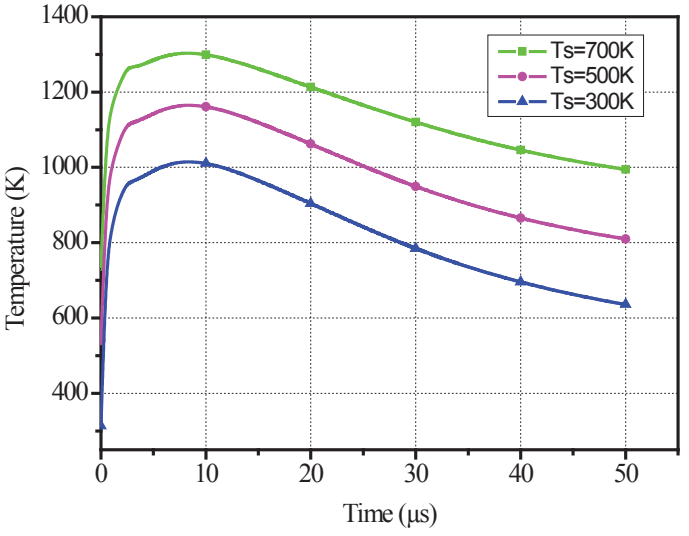


Figure 7: Variation of substrate surface temperature (0.5$\mu$m depth from the surface: z=-0.5$\mu$m) during the droplet spreading for different steel substrate initial temperatures (Ts=300K, Ts=500K, and Ts=700K)

Ts=300K, $\xi_{max}$=1.96 for Ts=500K, and $\xi_{max}$=1.98 for Ts=700K.

In this set of simulations, it was noticed that the final spread time is almost the same for all the substrate temperatures: it's about t=2$\mu$s. Consequently, the substrate temperature has a slight effect on the maximum spread factor and no effect on the maximum spread time.

The initial temperature of the substrate has also an influence on its maximum surface temperature reached after droplet impact. Figure 7 shows the temperature evolution at 0.5$\mu$m depth from the surface of a steel substrate during the droplet spreading for different initial substrate temperatures. The maximum surface temperature of the substrate, reached after droplet impact, increases with its initial temperature. It reaches a maximum of 1014K for Ts=300K, 1165K for Ts=500K and 1303K for Ts=700K. It can be expected from these data, that melting of the substrate surface may occur when increasing its initial temperature especially when using low melting point materials as substrate.

### *3.3 Effect of substrate material*

The nature of the substrate and therefore its thermo-physical properties also play an important role in droplet deposition and solidification process leading to splat formation. To investigate its influence, three different materials were used in simulations: steel, aluminum and alumina. The use of alumina as substrate will give an idea of the impact of a molten alumina droplet upon a previously solidified alumina splat. The thermal properties of these materials (conductivity, heat capacity and diffusivity) are listed in table 6. The spread factor evolution for different substrate materials is shown in figure 8, when initial substrate temperature is set to Ts=300K. The spread factor evolution is almost the same for all the substrate materials while its maximum value differs slightly from one material to another (1.92 for aluminum, 1.93 for steel and 1.95 for alumina).

The final spreading time is found to be almost the same for all substrates (t=2$\mu$s). The evolutions and final shapes of the droplet at the end of splat formation are similar to that shown in figure 2 (b) for steel substrate.

The substrate material affects the solidification time. Computed results resumed in Figure 5 show that the solidification time increases with the substrate temperature and that the effect is more important for alumina than for steel substrate, while the effect is weak for aluminum substrate.

The storage capacity of the material seems to be the parameter governing the substrate thermal effects. Hence, the splat cools down faster as the thermal inertia of the substrate material decreases (from alumina to aluminum).

Figure 9 shows the substrate temperature evolution at 1$\mu$m depth from the sur-

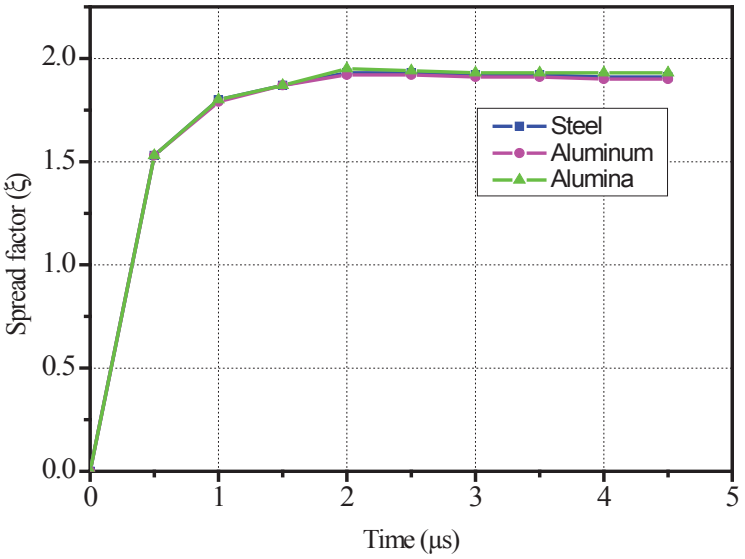


Figure 8: Evolution of the spread factor with time for different substrate materials: aluminum, steel and alumina (Ts=300K).

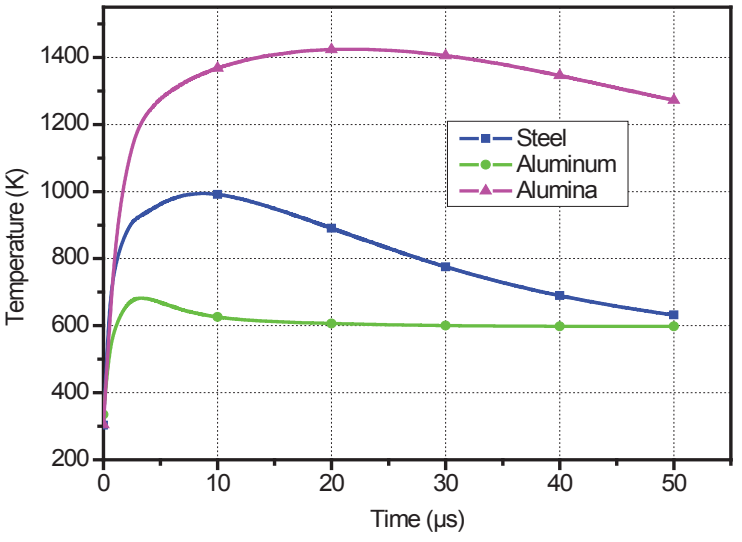


Figure 9: Evolution of the substrate temperature at 1$\mu$m depth from the surface (z=-1$\mu$m) during the alumina droplet deposition on different substrate materials for Ts=300K.

face (z=-1$\mu$m) during the alumina droplet deposition on different substrate materials. The substrate initial temperature was set to 300K. The maximum temperature reached at z=-1$\mu$m location and the corresponding time are reported in table 3.

It can be concluded from table 3 that as the thermal inertia of the substrate is higher, as it takes more time to cool down, therefore resulting in an increase of the splat solidification time. Table 4 resumes the computed values of the splat solidification time for various substrates at various initial temperatures.

Table 3: Maximum temperature reached, at 1$\mu$m depth from the substrate surface, and corresponding time, for different materials (Ts = 300K)

| Parameters / Material | ρ.Cp ($J/m^3.K$) | Maximal temperature reached (K) | Time (μs) |
|---|---|---|---|
| Alumina | 4132500 | 1424 | 21,5 |
| Steel | 3728750 | 994 | 8,5 |
| Aluminum | 2430000 | 682 | 3,5 |

### *3.4 Effect of thermal contact resistance*

During the droplet deposition, the contact between the droplet and the substrate is not perfect due to the roughness of the substrate surface and gas entrapment. This has an influence on the rate of heat transfer from the splat to the substrate and thus on the droplet deposition and solidification time. The non perfect contact is taken into account by introduction of a thermal contact resistance (TCR).

Computed results reported in Figure10 show the spread factor evolution during the droplet deposition on a steel substrate for different TCR values: $10^{-6}m^2K/W$, $5.10^{-7}m^2K/W$,$10^{-7}m^2K/W$ and $10^{-8}m^2K/W$. These values are the typical ones found in literature [Heichal and Chandra (2005), Bianchi (1995), Mebdoua, Y (2008)]. The initial temperature of substrate was set to 300K. The thermal contact resistance seems to have a significant effect on the deposition process: as the thermal contact resistance is increased, the maximum spread factor increases.

When the TCR is less than $10^{-7}m^2K/W$, no effect on the maximum spread factor was observed, but when the TCR exceeds $10^{-7}m^2K/W$, the maximum spread

factor increases. The time of complete solidification as a function of thermal contact resistance is shown in figure 11, as TCR is increased, the solidification time increases.

Table 4: Effect of initial temperature and material of substrate on splat solidification time.

| Substrate material | Initial substrate temperature (K) | Splat solidification time ($\mu$s) |
|---|---|---|
| Alumina | 300 | 34 |
| | 500 | 37.5 |
| | 700 | 42.5 |
| Steel | 300 | 21 |
| | 500 | 22.5 |
| | 700 | 26.5 |
| Aluminum | 300 | 18.5 |
| | 500 | 20 |
| | 700 | 22 |

The computed values of the maximum spread factor and the splat solidification time for various thermal contact resistances are resumed in table 5.

Indeed, increasing the contact resistance between the droplet and the substrate leads to a decrease in conduction rate, thus the droplet keeps its energy and then it takes more time to cool down and solidify thus allowing the splat to spread and reach a higher extent Decreasing TCR under $10^{-7}$m$^2$K/W value shows no further effects on the maximum spread factor and complete solidification time. Thus the contact between the droplet and the substrate may be considered perfect when the TCR is equal or less than $10^{-7}$m$^2$K/W.

Table 5: Effect of thermal contact resistance on the maximum spread factor and solidification time.

| TCR(m²K/W) / Parameters | $10^{-8}$ | $10^{-7}$ | $5.10^{-7}$ | $10^{-6}$ |
|---|---|---|---|---|
| Maximum spread factor | 1.93 | 1.93 | 2 | 2.2 |
| Splat solidification time (µs) | 18.5 | 21 | 30 | 34.7 |

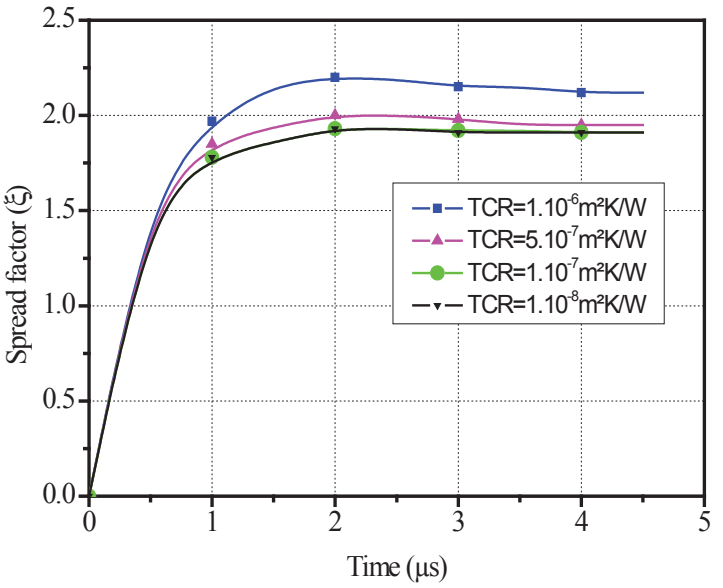


Figure 10: Effect of thermal contact resistance on the spread factor evolution during the droplet deposition on a steel substrate (Ts=300K).

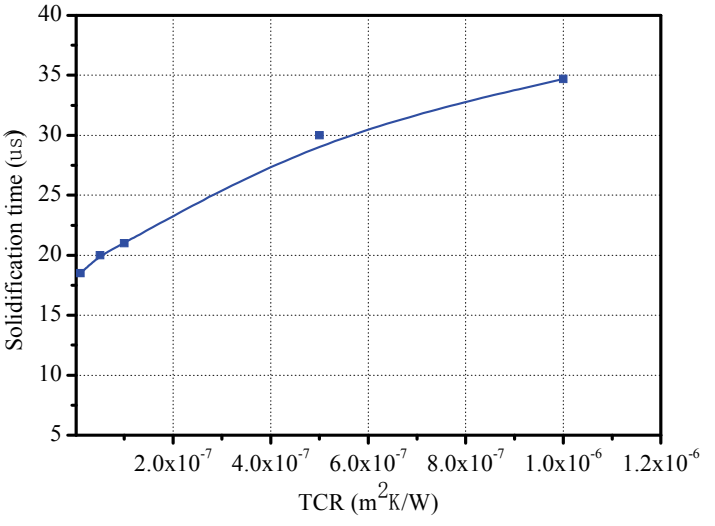


Figure 11: Variation of complete solidification time with thermal contact resistance during the droplet deposition on a steel substrate (Ts=300K).

Table 6: Thermophysical properties of materials used in this study.

| | Alumina | Air | Steel (AISI 4340) | Aluminum | Units |
|---|---|---|---|---|---|
| Density, $\rho$ | 2900 | 1.3 | 7850 | 2700 | $Kg/m^3$ |
| Viscosity, $\mu$ | $12.10^{-3}$ | $1.7\ 10^{-5}$ | - | - | Pa.s |
| Surface tension, $\sigma$ | 0.6 | | - | - | N/m |
| Thermal conductivity, $k$ | 5 | 0.0262 | 44.5 | 237 | W/(m.K) |
| Heat capacity, $Cp$ | 1425 | 1004 | 475 | 900 | J/(kg.K) |
| Diffusivity, $\alpha$ | $1.20\ 10^{-6}$ | $2.10^{-5}$ | $1.19\ 10^{-5}$ | $9.75\ 10^{-5}$ | $m^2/s$ |
| Latent heat of fusion, $\Delta H$ | 770 | - | - | - | kJ/kg |
| Thermal inertia ($\rho.Cp$) | 4132500 | - | 3728750 | 2430000 | $J/(m^3.K)$ |

## 4 Conclusion

In this paper, a numerical analysis was carried out to study the impact of a micrometric molten particle impacting onto a substrate using a Finite Element Analysis. The aim of this simulation was to investigate the influence of the key parameters that influence the droplet spreading and solidification process.

It was shown that substrate temperature and substrate material have a slight influence on the droplet spreading, while they have an important effect on the solidification time: increasing the substrate temperature or decreasing its thermal diffusivity, allows the splat to take more time to solidify and thus to spread more.

The thermal contact resistance has been found to have a great influence on the droplet solidification and the spread factor. Increasing the TCR leads to an increase both on the solidification time and on the maximum spread factor. The contact between the droplet and the substrate may be considered perfect when the TCR is equal or less than $10^{-7} m^2K/W$.

**Acknowledgement:** The authors would like to thank the AUF (French-speaking University Agency) and PHC Maghreb Hubert Curien project for supporting this work.

## References

**Bertagnolli, M; Marchese, M.; Jacucci, J.** (1995): Modeling of particles impacting on a rigid substrate under plasma spraying conditions, *J.Therm.Spray.Tech*, vol. 4, pp. 41-49.

**Bianchi. L.** (1995): Projection par Plasma d'arc et plasma inductif de dépôts Céramiques: Mécanismes de formation de la première couche et relation avec les propriétés mécaniques des dépôts". Thèse N° 95-41, Université de Limoges.

**Bianchi, L.; Blein, F.; Lucchese, P.; Vardelle, M.; Vardelle, A.; Fauchais. P.** (1994): Effect of particle velocity and substrate temperature on alumina and zirconia splat formation, *Thermal Spray Industrial Applications, (Ed.) C. C. Berndt et S. Sampath, (Pub.) ASM International, Material Park,* Oh, USA, pp.569-574.

**Bussmann, M.; Mostaghimi, J.; Chandra, S.** (1999): On a three dimensional volume tracking model of droplet impact, *Phys. Fluids*, vol. 11, pp. 1406–1417.

**Cedelle, J.; Vardelle, M.; Pateyron, B.; Fauchais, P.**(2005): Investigation of plasma sprayed coatings formation by visualization of droplet impact and splashing on a smooth substrate. *IEEE Transactions on Plasma Science,* vol. 33, no. 2, pp. 414-415.

**Celentano, D.; Cruchaga, M.; Romero, J.; El Ganaoui, M.** (2011) Numerical simulation of natural convection and phase-change in a horizontal Bridgman apparatus, *International Journal of Numerical Methods for Heat & Fluid Flow*, vol. 21, no. 4, pp. 366-376.

**Delluc, G.; Ageorges, H.; Pateyron, B.; Fauchais, P.**(2005): Fast modeling of plasma jet and particle behaviours in spray conditions. *High Temperature Material Processes,* vol. 9, no. 2, pp. 211-226.

**El Ganaoui, M.; Bontoux, P.; Morvan, D.** (1999): Localisation d'un front de solidification en interaction avec un bain fondu instationnaire. - *C. R. Acad. Sci. Paris, série IIb, t.*, vol. 327, pp. 41-48.

**El Ganaoui, M.; Lamazouade, A.; Bontoux, P.; Morvan, D.** (2002): Computational solution for fluid flow under solid/liquid phase change conditions, *Int. J. Computers and Fluids,* vol. 31, nos. 4-7, pp. 539-556.

**El Ganaoui, M.; Bontoux, P.** (1998): An homogenisation method for solid-liquid phase change during directional solidification, ASME, H.T.D., *Numerical and Experimental Methods in Heat Transfer,* éd. R.A. Nelson, T. Chopin, S.T. Thynell, vol. 361, no. 5, pp. 453-469.

**Ettouil, F.B.; Mazhorova, O.; Pateyron, B.; Ageorges, H.; El Ganaoui, M.; Fauchais, P.** (2008): Predicting dynamic and thermal histories of agglomerated particles injected within a d.c. plasma jet. *Surface and Coatings Technology*, vol.

202, no. 18, pp. 4491-4495.

**Fataoui. K.; Pateyron, B.; El Ganaoui, M.; Rhanim, Belafhal, A.** (2008): Simulation of the thermal history and induced mechanical stresses during a plasma spray coating process, 2008. *Phys. Chem. News*, vol. 40, pp. 23-28.

**Fauchais, P.; Fukumoto, M.; Vardelle, A.; Vardelle M.** (2003): Knowledge concerning splat formation: an invited review. *Journal of Thermal Spray Technology*, vol. 13, pp. 3, pp. 337-360.

**Fukai, J.; Shiiba, Y.; Yamamoto, T.; Miyatake, O.; Poulikakos, D., Megaridis, C.M.; Zhao, Z.** (1995): Wetting effects on the spreading of a liquid droplet colliding with a flat surface: experiment and modeling, *Physics of Fluids*, vol. 7, no. 2, pp. 236-247.

**Fukai, J.; Zhao, Z.; Poulikakos, D.; Megaridis, C.M.; Miyatake, O.** (1993): Modeling of the deformation of a Liquid droplet impinging upon a flat surface. *Phys. Fiuids*, vol. A 5, no. 11, pp.2588-2599.

**Fukumoto, M; Katoh, S; Okane, I; Ohmori, A.** (1995): Splat behavior of plasma sprayed particles on flat substrate surface, *Proceedings of 14th Int. Thermal Spray Conf., Kobe, ed.A.Ohmori, Japan High Temperature Society*, pp.353-358.

**Harlow, F.H.; Shannon, J.P.** (1967): The splash of a liquid droplet, *J. Appl. Phys.*, vol. 38, pp. 3855.

**Heichal, Y.; Chandra, S.** (2005):Predicting Thermal Contact Resistance between molten metal droplets and a solid surface. *J. of Heat Transfer*, vol. 127, no. 11, pp. 1269-1275.

**Hogea, C.S.; Murray, B.T.; Sethian, J.A.** (2005): Implementation of the level set method for continuum mechanics based tumor growth models, *FDMP: FDMP: Fluid Dynamics and Materials Processing*, vol. 1, no. 2, pp. 109-130.

**Ivosevic, M.; Richard, A.; Cairncross, B.; Knight, R.** (2006): 3D predictions of thermally sprayed polymer splats: Modeling particle acceleration, heating and deformation on impact with a flat substrate, *Intern Journal of Heat and Mass Transfer*, vol. 49, pp. 3285-3297.

**Liu, H; Lavernia, E.J.; Rangel, R.** (1993): Numerical simulation of substrate impact and freezing of droplets in plasma spray process, *J. Phys.D: Appl.Phys*, vol. 26, pp.1900-1998.

**Lowengrub, J.S.; Xu, J-J.; Voigt, A.** (2007): Surface Phase Separation and Flow in a Simple Model of Multicomponent Drops and Vesicles. *FDMP: Fluid Dynamics and Materials Processing*, vol. 3, no. 1, pp. 1-20.

**Madejski, J.** (1976): Solidification of droplets on a cold surface. *International Journal of Heat and Mass Transfer*, vol. 19, pp. 1009-1013.

**Mebdoua, Y.** (2008): Etude Numérique des Phénomènes Thermiques Contrôlant la Solidification d'une Lamelle en Projection Thermique : Application à la Formation du Dépôt, *thèse de l'université de Limoges*.

**Mundo, C.; Sommerfeld, M.; Tropea, C.**. (1995): Droplet-wall collisions. Experimental studies of the deformation and breakup process. *International Journal of Multiphase Flow*, vol. 21, no. 2, pp.l5l–l73.

**Oukach, S.; El Ganaoui, M; Hamdi, H.; Pateyron, B.** (2010): Deformation behavior of a liquid droplet impacting on a solid surface. *Proceeding of the 6th annual European COMSOL Conference*, November 17-19, Paris, France.

**Oukach, S.; Pateyron, B.; El Ganaoui, M.; Hamdi, H.** (2010): Simulation numérique de l'étalement d'une goutte sur une paroi. *Proceeding du 1er Congrès de l'Association Marocaine de Thermique (AMT 2010)*, 6 et 7 mai Settat, Maroc.

**Prud'homme, R.; El Ganaoui, M.** (2006): Solid/Liquid Phase Change: Recent Studies and Models. *FDMP: Fluid Dynamics and Material Processes*, vol.1, no.1, pp. 11-21.

**Pasandideh-Fard, M.; Mostaghimi, J.** (1994): Deformation and solidification of molten particles on a substrate in thermal plasma spraying. *Proceedings of the 7th National Thermal Spray Conference*, Boston, Massachusetts, pp. 405-414.

**Pasandideh-Fard, M; Mostaghimi, J.** (1996): On the Spreading and Solidification of Molten Particles in a Plasma Spray Process: Effect of the Thermal Contact Resistance. *Plasma Chemistry and Plasma Processing*. vol. 16, no. 1, pp. 83-98.

**Pateyron, B.; Delluc, G.; Calve, N.** (2005): T&T Winner, the chemistry of on-line transport properties in interval of 300 K to 20.000 K. *Mécanique et Industries.* vol. 6, no. 6, pp. 651-654.

**Pateyron, B.; Elchinger, M.F.; Delluc, G.; Fauchais, P.** (1996): Sound velocity in different reacting thermal plasma systems. *Plasma Chemistry and Plasma Processing*, vol. 16, no. 1, pp. 39-57.

**Sethian, J.** (1996): level Set Methods: Evolving Interfaces in Geometry, Fluid Mechanics, Computer Vision and Material Sciences. *Cambridge University Press*, Cambridge.

**Sikalo, S.; Tropea, C.; Ganic, E.N.** (2005): Impact of droplets onto inclined surfaces. *Journal of Colloid and Interface Science.* vol. 286, no. 2, pp. 661–669.

**Trapaga, G.; Matthys, E. F.; Valencia, J. J.; Szekely J.** (1992): Fluid flow, heat Transfer and solidification of molten metal droplets impinging on substrate: comparison of numerical and experimental results. *Metall. Trans.,* vol. 23B, pp. 701–718,

**Tsurutani, K.; Yao, M.; Senda, J.; Fujimoto, H.** (1990): Numerical analysis of

the deformation process of a droplet impinging upon a wall. *JSME Int. Ser. II*, vol. 33, pp. 555.

**Voller, V. R.; Markatos, N. and Cross, M.**. (1985): Techniques for accounting for the moving interface in convection /diffusion phase change. *Numerical Methods in Thermal Problems*, vol. 1, pp. 595–609.

**Worthington, A. M.** (1876): On the forms assumed by drops of liquids falling vertically on a horizontal plate, *Proc R Soc London A*; vol. 25, pp. 261-271.

**Worthington, A. M.** (1877): A second paper on the forms assumed by drops of liquids falling vertically on a horizontal plate. *Proc R Soc London A*, vol. 25, pp. 498-503.